Review Article Adv. Mat. Lett. 2013, **4**(7), 522-533 ADVANCED MATERIALS Letters

www.amlett.com, www.amlett.org, DOI: 10.5185/amlett.2012.9426 Published online by the VBRI press in 2013

Ferrolectric nanofibers: principle, processing and applications

Seema Sharma*

Department of Physics, A. N. College, Patna 800013, India

*Corresponding author. E-mail: seema_sharma26@yahoo.com

Received: 13 September 2012, Revised: 28 November 2012 and Accepted: 08 December 2012

ABSTRACT

Nanotechnology is one of the rapidly growing scientific disciplines due to its enormous potential in creating novel materials that have advanced applications. Electrospinning has been found to be a viable technique to produce materials in nanofiber form. Ferroelectric and/or piezoelectric materials in nanofiber and/or nanowire form have been utilized for producing energy harvesting devices, high frequency transducers, implanted biosensors, vibration absorbers and composite force sensors, etc. An in-depth review of research activities on the development of ferroelectric nanofibers, fundamental understanding of the electrospinning process, and properties of nanostructured fibrous materials and their applications is provided in this article. A detailed account on the type of fibers that have been electrospun and their characteristics is also elaborated. It is hoped that the overview article will serve as a good reference tool for nanoscience researchers in ferroelectric materials. Copyright © 2013 VBRI press.

Keywords: Nanofiber; electrospinning; energy harvesting; ferroelectric; perovskite.

Seema Sharma is Reader, Dept of Physics, A N College, Patna, India. She worked as Assistant Professoor at BITS Pilani-Goa campus for two years. She did her PhD in 1992 from IIT Kharagpur and did her post doctoral research at various institutes such as IIT Delhi, India, Lehigh University, Pennsylvania, USA, Manchester University, UK and IISC Bangalore, India. She has wide experience in the field of electroceramics and thin films, multiferroic nanostructured materials and Bionanomaterials. She has successfully handled sponsored and in-house research projects successfully and has published more than 80 research papers in international referred journals.

Introduction

Nanoscale materials are invariably used as memory devices, actuators, sensors, biomedical devices and are also required in many applications [**1-4**]. These requirements might be satisfied by nanoscale ferroelectric materials. In addition, these nanoscale materials also have the potential to be used for energy harvesting for wireless nano- and microdevices. One-dimensional (1D) nanostructures, such as nanowires, nanotubes, and nanofibers, represent the smallest dimension for efficient transport of electrons and excitons, and thus are ideal building blocks for hierarchical assembly of functional nanoscale electronic and photonic structures. Several ferroelectric and/or piezoelectric nanowires and nanofibers are very promising in making a great breakthrough [**4-7**]. For instance, zinc oxide, cadmium sulfide, Barium titanate, sodium potassium niobate and gallium nitride nanowires have been utilized in the conversion of mechanical energy to electric energy due to the piezoelectric effect of these materials. These ferroelectric nanowires and nanofibers can potentially be used for energy harvesting devices, high frequency transducers, implanted biosensors, vibration absorbers and composite force sensors, etc [**8, 9**]. Ferroelectric and/or Piezoelectric materials, especially in the form of low-dimensional nanostructures, own a number of advantages in micro-electro-mechanical systems (MEMS), such as low hysteresis, high available energy density, high sensitivity with wide dynamic range, and low power requirement,

therefore it is worth considering the impetus for integrating piezoelectric nanostructures into MEMS devices.

Various approaches have been used such as template based growth, chemical vapor deposition, and laser ablation. These methods, however, require multiple steps and therefore are cost and time consuming. Etching, template removal and purification are good examples. Also, especially for electronic applications, low throughput prevents these synthesis methods to be compatible with device fabrication. On the other hand, electrospinning has been demonstrated as a simple and versatile process for synthesizing complex oxide nanofibers. Electrospinning originated from conventional fiber spinning. The main difference of electrospinning is applying a high electric field (usually 3 kV/cm or higher) to a liquid precursor to synthesize nanofibers. Versatility of this process arises from the use of conventional sol-gel precursors. Details and physics of electrospinning have been studied intensively in the past and only a brief description is presented here. In the electrospinning of ceramic nanofibers, conventional sol-gel precursors are mixed with various kinds of polymers to increase the viscosity and loaded into a container with a metallic needle tip. High voltage, either positive or negative is applied to a metallic needle tip while the collector is grounded.

This review paper describes the process of transforming ceramic piezoelectric materials into nanofibers, which are strong but also provide more design flexibility, thus expanding the possible sensing and actuating and energy harvesting in electronic industries. As a nanoscale fiber, the materials are flexible and damage-resistant, much like how glass is light and strong in fiber form but brittle on a larger scale.

Principle of fabrication of nanofibers

Electrospinning fundamentals

Unlike conventional fiber spinning techniques (wet spinning, dry spinning, melt spinning, gel spinning), which are capable of producing polymer fibers with diameters down to the micrometer range, electrostatic spinning, or 'electrospinning' is a process capable of producing polymer fibers in the nanometer diameter range [**9**]. Electrospinning is a novel and efficient fabrication process that can be utilised to assemble fibrous polymer mats composed of fiber diameters ranging from several microns down to fibers with diameter lower than 100 nm (**Fig. 1**). This electrostatic processing method uses a high-voltage electric field to form solid fibers from a polymeric fluid stream (solution or melt) delivered through a millimeter-scale nozzle. Nanofibers are the ultra-fine solid fibers notable for their very small diameters (lower than 100 nm), their large surface area per unit mass and small pore size. Due to the inherent properties of the electrospinning process, which can control the deposition of polymer fibers onto a target substrate, nanofibers with complex, and seamless three-dimensional shapes could be formed. Construction of nanoscale composite fibers by electrospinning from a mixture of rigid rod polymers and flexible polymers is also feasible. The electrospun nanofibers can even be aligned to construct unique functional nanostructures such as nanotubes and nanowires. Furthermore, depending on the specific polymer being used, a wide range of fabric properties such as strength, weight and porosity, surface functionality etc can be achieved. This novel fiber spinning technique provides as well the capacity to lace together a variety of types of polymers, fibers, and particles to produce ultra thin layers. Small insoluble particles can be added to the polymer solution and encapsulated in the dry nanofibers. Soluble drugs or bacterial agents can be added and electrospun into nonwoven mats. Although the process of electrospinning has been known for almost 70 years and the first patent was issued to Formhals in 1934 (US Patent, 1-975-504), polymeric nanofibers produced by electrospinning have become a topic of great interest for the past few years [**10**].

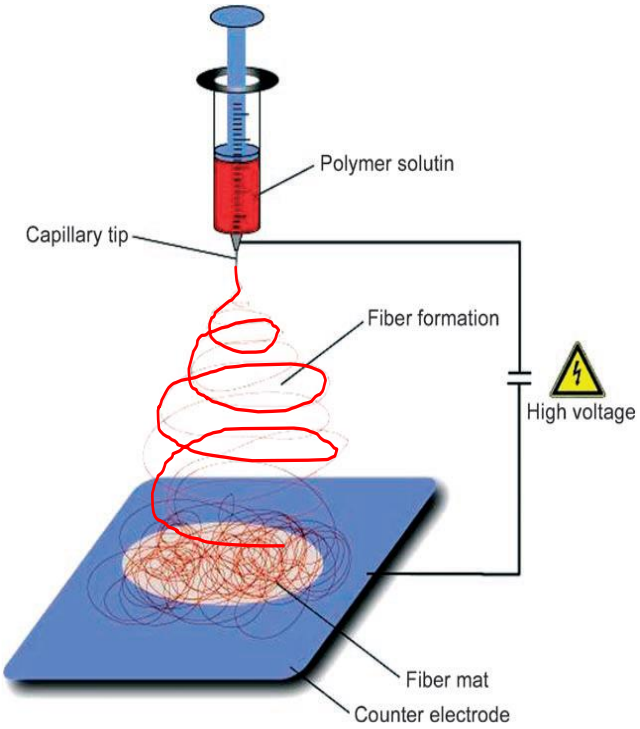

Fig. 1. Basic setup for an electrospinning experiment with a perpendicular arrangement of the electrodes.

Electrospun nanofibers could be collected as single fibers, nonwoven mats, uniaxially aligned arrays, or multilayered films by modifying the electrospinning setup. In addition to controlling macroscopic organization of nanofibers, electrospinning allows one to maneuver the secondary structures of individual fibers as well as to increase their structural complexity. To this end, nanofibers with core/sheath, hollow, or porous structures have been produced by using specially designed spinnerets or adjusting the spinning parameters.

Typically, electrospinning is applicable to a wide range of polymers like those used in conventional spinning, i.e. polyolefine, polyamides, polyester, aramide, acrylic as well as biopolymers like proteins, DNA, polypeptides, or others like electric conducting and photonic polymers [**11-13**]. The high specific surface area and small pore size of electrospun nanofibers make them interesting candidates for a wide variety of applications. Another interesting aspect of using electrospun fibers is that the fibers may

dissipate or retain the electrostatic charges depending on the electrical properties of the polymer. The charges can be manipulated as well by electrical fields and the electrical polarity of the fibers is affected by the polarity of the applied voltage [**14-17**]. Nanofibers provide also a connection between the nanoscale world and the macroscale world, since the diameters are in the nanometer range and the lengths are kilometres.

Many new electrospinning techniques have appeared, such as vibration electrospinning, magneto-electrospinning, Siroelectrospinning and bubble electrospinning [**18, 19**]. Nanotechnology bridges the gap between deterministic laws (Newtonian mechanics) and probabilistic laws (quantum mechanics). The nano-effect has been demonstrated for unusual strength, high surface energy, surface reactivity and high thermal and electric conductivity. It is a challenge to develop technologies capable of preparing nanofibers with diameters under 100nm without beads, especially for smaller nanofibers. At such a small scale, it is very important to avoid the occurrence of beads. Beads are considered as the main demerit of the electrospun fibers. There are many factors affecting the occurrence of beads, such as applied voltage, viscoelasticity of the solution, charge density and surface tension of the solution. Much attention has been directed towards the formation and morphology of beads in electrospun products. However, the mechanism for the formation of beads is still unknown and little research on this has been performed so far. The methods to reduce the numbers and sizes of beads are by adjusting weight concentrations, adding salt additives and variation of the solvent. Controlling the concentrations of polymer solutions and salt additives could prevent beads from occurring in the electrospinning process, and solvents could also affect the number and morphology of beads and also the size of the electrospun fibers.

History of electrospinning

The origin of electrospinning as a viable fiber spinning technique can be traced back to the early 1930s. In 1934, Formhals patented his first invention relating to the process and the apparatus for producing artificial filaments using electric charges. Though the method of producing artificial threads using an electric field had been experimented with for a long time, it had not gained importance until Formhals's invention due to some technical difficulties in earlier spinning methods, such as fiber drying and collection [**10**]. Formhals's spinning process consists of a movable thread collecting device to collect the threads in a stretched condition, like that of a spinning drum in the conventional spinning. Formhals's process was capable of producing threads aligned parallel on to the receiving device in such a way that it can be unwound continuously. In his first patent, Formhals reported the spinning of cellulose acetate fibers using acetone as the solvent. The first spinning method adopted by Formhals had some technical disadvantages. It was difficult to completely dry the fibers after spinning due to the short distance between the spinning and collection zones, which resulted in a less aggregated web structure. In a subsequent patent, Formhals refined his earlier approach to overcome the aforementioned drawbacks. In the refined process, the distance between the feeding nozzle and the fiber collecting device was altered to give more drying time for the electrospun fibers.

Subsequently in 1940, Formhals patented another method for producing composite fiber webs from multiple polymer and fiber substrates by electrostatically spinning polymer fibers on a moving base substrate. In the 1960s, fundamental studies on the jet forming process were initiated by Taylor. In 1969, Taylor studied the shape of the polymer droplet produced at the tip of the needle when an electric field is applied and showed that it is a cone and the jets are ejected from the vertices of the cone. This conical shape of the jet was later referred to by other researchers as the "Taylor Cone" in subsequent literature. By a detailed examination of different viscous fluids, Taylor determined that an angle of 49.3 degrees is required to balance the surface tension of the polymer with the electrostatic forces. The conical shape of the jet is important because it defines the onset of the extensional velocity gradients in the fiber forming process. In subsequent years, focus shifted to studying the structural morphology of nanofibers. Researchers were occupied with the structural characterization of fibers and the understanding of the relationships between the structural features and process parameters. Wide-angle X-ray diffraction (WAXD), scanning electron microscopy (SEM), transmission electron microscopy (TEM), and differential scanning calorimetry (DSC) have been used by researchers to characterize electrospun nanofibers. In 1971, the electrospinning of acrylic microfibers were done whose diameters ranged from 500 to 1100 nm. Limits of spinability of a polyacrylonitrile/dimethylformamide (PAN/DMF) solution were determined and a specific dependence of fiber diameter on the viscosity of the solution was observed. It was also shown that the diameter of the jet reached a minimum value after an initial increase in the applied field and then became larger with increasing electric fields [20-22]. Polyethylene and polypropylene fibers were produced from the melt, which were found to be relatively larger in diameter than solvent spun fibers. The relationship between the fiber diameters and melt temperature showed that the diameter decreased with the increasing melt temperature. According to this, fiber diameter reduced by 50% when the applied voltage doubled, showing the significance of applied voltage on fiber characteristics. In 1987, the effects of electric field, experimental conditions, and the factors affecting the fiber stability and atomization were studied. It was concluded that liquid conductivity plays a major role in the electrostatic disruption of liquid surfaces. Highly conducting fluids with increasing applied voltage produced highly unstable streams that whipped around in different directions. Relatively stable jets were produced with semi conducting and insulating liquids, such as paraffinic oil. It was also showed that unstable jets produce fibers with broader diameter distribution. After a hiatus of a decade or so, a major upsurge in research on electrospinning took place due to increased knowledge on the application potential of nanofibers in different areas, such as high efficiency filter media, protective clothing, catalyst substrates, and adsorbent materials. The characteristics of polyethylene oxide (PEO) nanofibers were studied by varying the solution concentration and applied electric

potential [**4-7**]. Jet diameters were measured as a function of distance from the apex of the cone, and they observed that the jet diameter decreases with the increase in distance. They found that the PEO solution with viscosity less than 800 centipoise (cP) was too dilute to form a stable jet and solutions with viscosity more than 4000 cP were too thick to form fibers. The thinning of fibers resulted as the extrusion progressed in PEO/water electrospun fibers. An increase in the applied voltage changes the shape of the surface from which the jet originates and the shape change has been correlated to the increase in the bead defects. A rigorous work was pursued on the experimental characterization and evaluation of fluid instabilities, which are crucial for the understanding of the electrospinning process. New apparatus were designed that could give enough control over the experimental parameters to quantify the electrohydrodynamics of the process. It was shown that the Ostwalt–deWaele power law could be applied to the electrospinning process. Study on the transport properties of electrospun fiber mats showed that nanofiber layers give very less resistance to the moisture vapor diffusional transport.

Electrospinning theory and process

Electrospinning is a unique approach using electrostatic forces to produce fine fibers [**18**]. Electrostatic precipitators and pesticide sprayers are some of the well known applications that work similarly to the electrospinning technique. Fiber production using electrostatic forces has invoked glare and attention due to its potential to form fine fibers. Electrospun fibers have small pore size and high surface area. There is also evidence of sizable static charges in electrospun fibers that could be effectively handled to produce three dimensional structures. Electrospinning is a process by which a polymer solution or melt can be spun into smaller diameter fibers using a high potential electric field. This generic description is appropriate as it covers a wide range of fibers with submicron diameters that are normally produced by electrospinning. Based on earlier research results, it is evident that the average diameter of electrospun fibers ranges from 100 nm–500 nm. In textile and fiber science related scientific literature, fibers with diameters in the range 100 nm–500 nm are generally referred to as nanofibers. The advantages of the electrospinning process are its technical simplicity and its easy adaptability. The apparatus used for electrospinning is simple in construction, which consists of a high voltage electric source with positive or negative polarity, a syringe pump with capillaries or tubes to carry the solution from the syringe or pipette to the spinnerette, and a conducting collector like aluminum. The collector can be made of any shape according to the requirements, like a flat plate, rotating drum, etc. A schematic of the electrospinning process is shown in **Fig. 1**.

Many researchers have used an apparatus similar to the one given in **Fig. 1** with modifications depending on process conditions to spin a wide variety of fine fibers. Polymer solution or the melt that has to be spun is forced through a syringe pump to form a pendant drop of the polymer at the tip of the capillary. High voltage potential is applied to the polymer solution inside the syringe through an immersed electrode, thereby inducing free charges into the polymer solution. These charged ions move in response to the applied electric field towards the electrode of opposite polarity, thereby transferring tensile forces to the polymer liquid. At the tip of the capillary, the pendant hemispherical polymer drop takes a cone like projection in the presence of an electric field. And, when the applied potential reaches a critical value required to overcome the surface tension of the liquid, a jet of liquid is ejected from the cone tip. Most charge carriers in organic solvents and polymers have lower mobilities, and hence the charge is expected to move through the liquid for larger distances only if given enough time.

After the initiation from the cone [**5**], the jet undergoes a chaotic motion or bending instability and is field directed towards the oppositively charged collector, which collects the charged fibers. As the jet travels through the atmosphere, the solvent evaporates, leaving behind a dry fiber on the collecting device. For low viscosity solutions, the jet breaks up into droplets, while for high viscosity solutions it travels to the collector as fiber jets.

Electrospinning: Jet initiation

The behavior of electrically driven jets, the shape of the jet originating surface, and the jet instability are some of the critical areas in the electrospinning processes. Sir Geoffrey Ingram Taylor in 1964 described this phenomenon, theoretically derived based on general assumptions that the requirements to form a perfect cone under such conditions required a semi-vertical angle of 49.3° (a whole angle of 98.6°) and demonstrated that the shape of such a cone approached the theoretical shape just before jet formation. He showed that a conical shaped surface referred to as the Taylor cone (**Fig. 2**) (A Taylor cone refers to the cone observed in electrospinning, electrospraying and hydrodynamic spray processes from which a jet of charged particles emanates above a threshold voltage) with an angle of 49.3° is formed when a critical potential is reached to disturb the equilibrium of the droplet at the tip of the capillary, that is, the initiating surface. When a high potential is applied to the solution, electrical forces and the surface tension help in creating a protrusion wherein the charges accumulate. The high charge per unit area at the protrusion pulls the solution further to form a conical shape, which on further increase in the potential initiates the electrospinning process by jetting [**18**]. Taylor cone corresponds only to a specific self-similar solution and there exists another shape corresponding to non self similar solutions. It has been shown both experimentally and theoretically that a liquid surface on application of a critical electric potential forms a conical shape with an angle of 33.5°, that is, less than the typical Taylor cone angle of 49.3°. Different shapes of the jet initiation have been associated with varying degrees of instability along the path of the jet. (Taylor cone formation: When a small volume of electrically conductive liquid is exposed to an electric field, the shape of liquid starts to deform from the shape caused by surface tension alone. As the voltage is increased the effect of the electric field becomes more prominent and as it approaches exerting a similar amount of force on the droplet as the surface tension does a cone shape begins to form with convex sides and a rounded tip. This approaches the shape of a cone with a whole angle (width) of 98.6°.

When a certain threshold voltage has been reached the slightly rounded tip inverts and emits a jet of liquid [**6, 7**]. This is called a cone-jet and is the beginning of the electrospraying process in which ions may be transferred to the gas phase. It is generally found that in order to achieve a stable cone-jet a slightly higher than threshold voltage must be used. As the voltage is increased even more other modes of droplet disintegration are found. The term Taylor cone can specifically refer to the theoretical limit of a perfect cone of exactly the predicted angle or generally refer to the approximately conical portion of a cone-jet after the electrospraying process has begun.

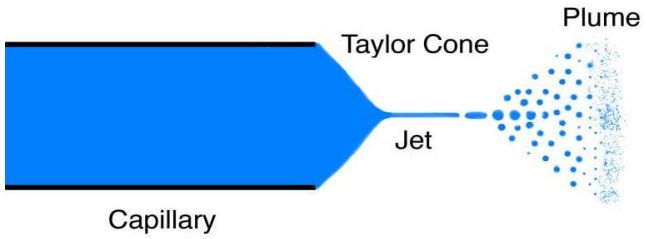

Fig. 2. Schematic diagram of the formation of the taylor cone during the elctrospinning process.

Process parameters and fiber morphology

Applied voltage

Various instability modes that occur during the fiber forming process are expected to occur by the combined effect of both the electrostatic field and the material properties of the polymer. The onset of different modes of instabilities in the electrospinning process depends on the shape of the jet initiating surface and the degree of instability, which effectively produces changes in the fiber morphology [**4**]. In electrospinning, the charge transport due to the applied voltage is mainly due to the flow of the polymer jet towards the collector, and the increase or decrease in the current is attributed to the mass flow of the polymer from the nozzle tip. The change in the spinning current is related to the change in the instability mode. It was experimentally showen that an increase in applied voltage causes a change in the shape of the jet initiating point, and hence the structure and morphology of fibers [**18**]. Experimentation on a PEO/water system has shown an increase in the spinning current with an increase in the voltage. It was also observed that for the PEO/water system, the fiber morphology changed from a defect free fiber at an initiating voltage of 5.5 kV to a highly beaded structure at a voltage of 9.0 kV. The occurrence of beaded morphology has been correlated to a steep increase in the spinning current, which controls the bead formation in the electrospinning process. Beaded structure reduces the surface area, which ultimately influences the filtration abilities of nanofibers. A two-electrode setup was used for electrospinning, by introducing a ring electrode in between the nozzle and the collector. The ring electrode was set at the same potential as the electrode immersed in the polymer solution. This setup was thought to produce a field-free space at the nozzle tip to avoid changes in the shape of the jet initiating surface due to varied potential [**19**]. Though this setup reduces the unstable jet behavior at the initiation stage, bending instability is still dominant at later stages of the process, causing an uneven chaotic motion of the jet before depositing itself as a nonwoven matrix on the collector. Another new electrospinning apparatus was used by introducing eight copper rings in series in between the nozzle and the collector for dampening the bending instability. The nozzle and the ring set were subjected to different potentials (ring set at a lower potential) of positive polarity, while the collector was subjected to a negative polarity. The idea behind this setup was to change the shape of the macroscopic electric field from the jet initiation to the collection target in such a way that the field lines converge to a center line above the collection target by the applied potential to the ring electrodes. The bending instability of fibers was dampened by the effect of the converging field lines producing straight jets. Controlled deposition helps to produce specific deposition patterns and also yarn like fibers. The spinning of PEO in aqueous solution was investigated using multiple electric fields, which resulted in fibers depositing over a reduced area due to the dampening of bending instability. The multiple field technique was also shown to produce fibers of lesser diameter than the conventional electrospinning method.

Polymer flow rate

The flow rate of the polymer from the syringe is an important process parameter as it influences the jet velocity and the material transfer rate. In the case of PS fibers, it was observed that the fiber diameter and the pore diameter increased with an increase in the polymer flow rate. As the flow rate increased, fibers had pronounced beaded morphologies and the mean pore size increased from 90 to 150 nm [**22**].

Spinning environment

Environmental conditions around the spinneret, like the surrounding air, its relative humidity (RH), vacuum conditions, surrounding gas, etc., influence the fiber structure and morphology of electrospun fibers. It was observed that acrylic fibers spun in an atmosphere of relative humidity more than 60% do not dry properly and get entangled on the surface of the collector. The breakdown voltage of the atmospheric gases is said to influence the charge retaining capacity of the fibers. A new mechanism for pore formation by evaporative cooling called “breathe figures” was proposed. Breathe figures occur on the fiber surfaces due to the imprints of condensed moisture droplets caused by the evaporative cooling of moisture in the air surrounding the spinneret. The pore characteristics of polymer nano-fibers at varied RH emphasized the importance of phase separation mechanisms in explaining the pore formation of electrospun fibers [**23**].

Solution parameters and fiber morphology

Solution concentration

Solution concentration decides the limiting boundaries for the formation of electrospun fibers due to variations in the viscosity and surface tension. Low concentration solution forms droplets due to the influence of surface tension, while higher concentration prohibits fiber formation due to higher

viscosity [**24**]. By increasing the concentration of polystyrene solution, the fiber diameter increased and the pore size reduced to a narrow distribution. In the case of a PEO/water system, a bimodal distribution in fiber diameter was observed at higher concentrations. In the PEO system, average fiber diameter and the solution concentration were related to by a power law relationship. Undulating morphologies in fibers were attributed to the delayed drying and the stress relaxation behavior of the fibers at lower concentrations. As is evident from the discussions, the concentration of the polymer solution influences the spinning of fibers and controls the fiber structure and morphology.

Solution conductivity

Polymers are mostly conductive, with a few exceptions of dielectric materials, and the charged ions in the polymer solution are highly influential in jet formation. The ions increase the charge carrying capacity of the jet, thereby subjecting it to higher tension with the applied electric field [**25, 26**]. The jet radius varied inversely as the cube root of the electrical conductivity of the solution. Researchers demonstrated the effect of ions by adding ionic salt on the morphology and diameter of electrospun fibers. It was found that PDLA fibers with the addition of ionic salts like KH2PO4, NaH2PO4, and NaCl produced beadless fibers with relatively smaller diameters ranging from 200 to 1000 nm.

Volatility of solvent

As electrospinning involves rapid solvent evaporation and phase separations due to jet thinning, solvent vapor pressure critically determines the evaporation rate and the drying time. Solvent volatility plays a major role in the formation of nanostructures by influencing the phase separation process [**27**]. It was found that the use of highly volatile solvents like dichloromethane yielded PLLA fibers with pore sizes of 100 nm in width and 250 nm in length along the fiber axis. The effect of volume ratio of the solvent on the fiber diameter and morphology of electrospun PVC fibers was evaluated and it was found that the average fiber diameters decreased with an increase in the amount of DMF in the THF/DMF mixed solvent. I was also found that the electrolytic nature of the solvent to be an important parameter in electrospinning. The characteristics of electrospun fibers with respect to the physical properties of solvents were studied. The influence of vapor pressure was evident when PS fibers spun with different THF/DMF combinations resulted in micro and nanostructure morphologies at higher solvent volatility and a much diminished microstructure at lower solvent volatility.

The morphology of polycarbonate (PC) nanofibers was studied by optical and scanning electron microscope [**28**]. It was observed that morphology of fibers depends upon the concentration of PC or viscosity of the solution, vapor pressure and diffusion coefficient of solvent. Tetrahydrofuran (THF) easily diffuses with polymer, at higher concentration of PC and at higher flow rate of solution; fibers of micron size are formed because of high vapor pressure of THF. On the other hand, in case of mixed solvents (DMF and THF), by controlling processing parameters nanofibers of diameter up to 200 nm were fabricated.

Ferroelectrics in nanofiber form

Oxide materials have been emerging rapidly over the last 5 years. Among the ternary crystal structures, the perovskite structure (ABX_3) is the most multifunctional, as the functional properties can easily be tailored by chemical substitution [**28**]. Perovskite oxides (ABO_3) possess unique electronic, magnetic, and optical properties, including ferroelectricity, high-temperature superconductivity, and colossal magnetoresistance. The ideal (cubic) perovskite structure consists of corner-sharing oxygen-octahedra with the B cation in the center, and with the A cation in the 12-coordinated position between 8 octahedra. The three main classes of perovskites are $A^{I}B^{V}O_3$, $A^{II}B^{IV}O_3$, and $A^{III}B^{III}O_3$, with the Roman numerals depicting the valence state of the cations. Solid solutions between these three are also possible giving mixed valence state on both A and B site. Several of the perovskites are ferroelectric, which means that they have a spontaneous electric polarization that can be switched by an external electric field. Ferroelectricity is closely related to piezoelectricity and pyroelectricity; all ferroelectrics are also piezoelectric and pyroelectric, but not all piezoelectrics are pyroelectric, and not all pyroelectrics are ferroelectric. The prototype ferroelectric perovskite is $BaTiO_3$. The ferroelectricity in $BaTiO_3$ arises from a displacement of the titanium ion in the [001] direction of the tetragonal perovskite structure and $BaTiO_3$ is therefore labeled a displacive ferroelectric. At high temperature, $BaTiO_3$ has a paraelectric cubic perovskite structure (**Fig. 3a**). At 120°C, it transforms from the cubic phase to a ferroelectric tetragonal phase (**Fig. 3b, c**).

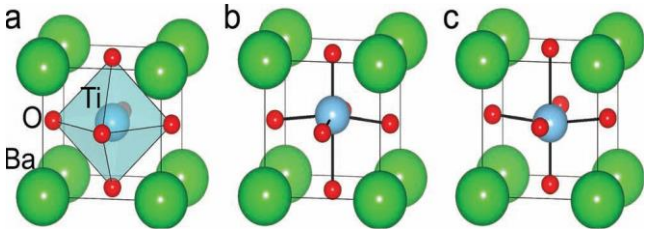

Fig. 3. Crystal structure of $BaTiO_3$, a) High-temperature paraelectric cubic phase. b,c) Room-temperature ferroelectric tetragonal phase, showing up and down polarization variants. The atomic displacements are scaled up to be clearly visible.

However, through the investigation of the phase transformations in barium titanate nanofibers, the Curie temperature increased significantly to a higher value (which is induced by the smaller internal stresses, resulting from the smaller grain size.) compared with that of bulk materials, which is crucial for the application of the $BaTiO_3$ ceramics in the high-temperature circumstance. The PFM piezoresponse of $BaTiO_3$/PVDF two-phase composite fibers ($BaTiO_3$ fiber within PVDF matrix) showed characteristic polarization-voltage and amplitude-voltage hysteresis loops, confirming their ferroelectric switching and piezoelectric hysteresis behaviours [**29, 30**].

Among the ferroelectrics there are a few important material classes that closely resemble the perovskites and which therefore will be included here: $LiNbO_3$ and layered oxide ferroelectrics. $LiNbO_3$ has a rhombohedral unit cell with a structure composed of oxygen octahedra containing the B atom and surrounded by the A atoms. Compared to the perovskite structure, the oxygen octahedra have been rotated around [111], such that the A atoms only have 6 oxygen first neighbors, rather than 12 as in the cubic perovskite structure. The layered oxide ferroelectrics belong to the family of Aurivillius compounds with a general formula $(Bi_2O_2)_2 + (Am - 1\ Bm\ O_{3m+1})^{2-}$, consisting of *m* perovskite-like blocks sandwiched between bismuth oxide layers where the A ion is Na, Sr, Ca, Ba, Pb, or Bi, the B ion is Ti, Ta, or Nb, and *m* can be an integer or half-integer. Examples include $SrBi_2Ta_2O_9$ (m = 2) and $Bi_4Ti_3O_{12}$ (m = 3). Among the Bismuth-layer-structured ferroelectrics, lanthanide-modified bismuth titanates ($Bi_{4x}R_xTi_3O_{12}$, R = La, Ce, Nd, Eu, etc) are regarded as very important candidates for NvFeRAM applications because of their larger remanent polarization, fast switching speed, excellent electrical properties, and lead-free nature. The piezoelectric, ferroelectric and dielectric characteristics suggest that Ce modified $Bi_4Ti_3O_{12}$ nanofibers may be well suited for realization of nanoscale piezoelectric devices as well as lead-free nonvolatile memory devices. In addition, multiferroic composites composed of nanoparticles of a ferroelectric oxide and nanoparticles of a ferromagnetic oxide are also there.

Advances in science and technology of ferroelectrics the last decade have resulted in the development of nanoscale ferroelectric structures and devices (<100 nm). Scaling of the device dimensions to the range where ferroelectrics start to show pronounced size effects has emphasized the importance of studies of ferroelectric properties at the nanoscale. When the physical dimensions of ferroelectric structures are reduced, the size effect is observed by a decrease in the remanent polarization, dielectric permittivity and phase transition temperature, increase in the coercive field, changes in the domain structure, etc. The ferroelectric size effect in 1D nanostructures has been much less studied compared to nanoparticles and thin fi lms [**31**]. This is largely because of the difficulty in producing high-quality ferroelectric 1D nanostructures with controllable dimensions and crystallinity. Until a decade ago, few 1D nanostructures of ferroelectric perovskites had been synthesized, only sub-micrometer- or micrometer-sized structures had been made.

There is an important class of phenomena that has not been exploited in ferroelectric polymers for electromechanical applications: the large lattice strain and large dimensional change associated with phase transformations in these materials. One such example is poly(vinylidene fluoride), PVDF, and its random copolymer with trifluoroethylene, P(VDF-TrFE), which are the best known and most widely used ferroelectric polymers. PVDF and its copolymer P(VDF-TrFE) are semicrystalline polymers that have a morphology of crystallites in an amorphous surrounding. With proper sample treatments a ferroelectric phase (β phase, which has an all-trans conformation can be induced in these polymers in the crystalline region. In compositions of P (VDF-TrFE) copolymers exhibit a ferroelectric-paraelectric transition (conversion of all-trans chains to a mixture of trans and gauche bonds), large lattice strains and sample dimensional changes (<10%). They belong to an important family of functional materials which have thermodynamically stable spontaneous polarization states switchable by application of a sufficiently strong external electric field. Studies on ferroelectric polymers are increasingly motivated by their exceptionally excellent dielectric, piezoelectric, pyroelectric, ferroelectric, and electro-optic properties. Their versatile applications include high density arrays of capacitors, light switches or displays, piezoelectric or pyroelectric sensors, thin-film transistors, and non-volatile memories. P (VDF-TrFE)s have shown great promise as electroactive polymers that can efficiently convert electrical energy into mechanical energy. They provide opportunities for fabricating ferroelectric polymer actuators for artificial muscles, Braille display, image processing, and microelectromechanical systems (MEMS). The storage and movement of electrical charges is fundamental to the electrical and electromechanical responses of electroactive polymers. Therefore, current trends lean toward developing polymers with high electric energy densities, which are dependent on dielectric constant and applied field strength. As spontaneously polarized materials, ferroelectric polymers have a much higher dielectric constant than other dielectric polymers for commercial use and can tolerate a high electric field to induce permanent polarization. Nevertheless, their energy densities alone are barely enough to meet the requirements of advanced applications. Micrometer-sized particles of ceramics, metals, organic semiconductors, and conductive polymers provide ferroelectric polymer 0–3 type composites with a rather high dielectric constant at weak fields. One may follow several criteria to design high dielectric constant ferroelectric polymer composites for electromechanical devices. First, the second phase added into the ferroelectric polymers should be flexible enough to achieve a high actuation strain of the composites. Second, low volume fractions of the fillers may be used to avoid their excessive agglomeration, which is adverse to their electric behaviour under high field strength. Conductive nanofibers enhance the electric properties of ferroelectric polymers. Polyaniline (PANI) nanofibers doped by protonic acids have a high dispersion stability in vinylidene fluoride-trifluoroethylene copolymers [P (VDF-TrFE)] and lead to percolative nanocomposites with enhanced electric responses. About a 50-fold rise in the dielectric constant of the ferroelectric polymer matrix has been achieved. Percolation thresholds of the nanocomposites are relevant to doping levels of PANI nanofibers and can be as low as 2.9wt% for fully doped nanofibers. The interface between the conductive nanofiber and the polymer matrix plays a crucial role in the dielectric enhancement of the nanocomposites in the vicinity of the percolation threshold. Compared with other dopants, perfluorosulfonic acid resin is better at improving the performance of the nanofibers in that it serves as a surface passivation layer for the conductive fillers and suppresses leakage current at low frequency. The nanofibers drastically reduce the electric field strength required to switch spontaneous polarization of P(VDF-TrFE). These nanofibers can be utilized for potential

applications as high energy density capacitors, thin-film transistors, and non-volatile ferroelectric memories. The particles in host polymers are another important factor to tailor properties of the composites. Fillers with elongated shapes have more opportunities to contact with each other to form continuous paths in the composites. The size of the fillers should also be taken into consideration in view that interface interactions between two phases are notable in fine particles. Interfacial exchange coupling mechanisms gives rise to marked dielectric enhancement when the fillers keep shrinking toward the nanometer scale. Nanoparticles usually perform their functions at volume contents as low as a few percentage. In comparison, much higher loadings (15–60%) of micrometersized particles are required to give the same performance. The conductive polyaniline (PANI) nanofibers are valuable enhancers of the electric properties of composites. PANIs have an inherent advantage in their ability to adjust conductivities by very simple inorganic/organic acid doping or base dedoping processes soon after polymerization. They can vary from insulators to conductors by controlling the degree of protonation. It is of utmost importance to consider the conductivities of filler phases and their interfacial interactions with ferroelectric polymer phases, because both of them will be eventually proven here to afford composites with variable capabilities. Since PANI nanofibers have been readily prepared through interfacial polymerization, they are ideal materials to optimise performance of the 1–3 ferroelectric polymer nanocomposites. A nanofibrous shape is one of the structures that enables long-range migration of electronic carriers along the fiber axis and gives rise to fillers with giant polarization. The intrinsically large surface area-to-volume ratio of the conductive nanofibers leads to a high charge capacity at the PANI–matrix interface. A short distance for electron transport perpendicular to the nanofibers will bring about ultrafast charge/discharge rates of the ferroelectric polymer composite capacitors and instant electric-induced strain of electromechanical devices. Ceramic PZT and polymeric PVDF are two piezoelectric materials which have been demonstrated as viable nanofiber nanogenerator materials [**31-35**]. In these efforts, either near-field electrospinning (NFES) or the conventional far-field electrospinning (FFES) process has been the key manufacturing tool to produce nanofibers. For the NFES process, a continuous single nanofiber can be deposited in a controllable manner, while the FFES process can produce dense nanofibers networks on large areas for the nanogenerator demonstrations. In general, a poling process, consisting of both electrical poling and mechanical stretching, is required in the fabrication of materials with piezoelectric properties at moderate temperature. Given the high electrostatic field and polymer jet characteristics of the electrospinning process, electrospinning is ideally suited for producing piezoelectric nanofibers through in-situ electric poling and mechanical stretching.

PVDF has superior piezoelectric properties as compared with other types of polymeric materials due to its polar crystalline structure. In nature, PVDF polymer consists of at least five different structural forms depending on the chain conformation of trans(T) and gauche (G) linkages. **Fig. 4**(a) shows the crystalline structure of the α and β-phase, respectively. While the α -phase is known as the most abundant form in nature, β-phase is responsible for most of PVDF's piezoelectric response due to its polar structure with oriented hydrogen and fluoride(CH_2–CF_2) unit cells along with the carbon backbone. In order to obtain the β-phase PVDF, electrical poling and mechanical stretchin gprocesses are required during the manufacturing process to align the dipoles in the crystalline PVDF structures as illustrated in **Fig. 4.**

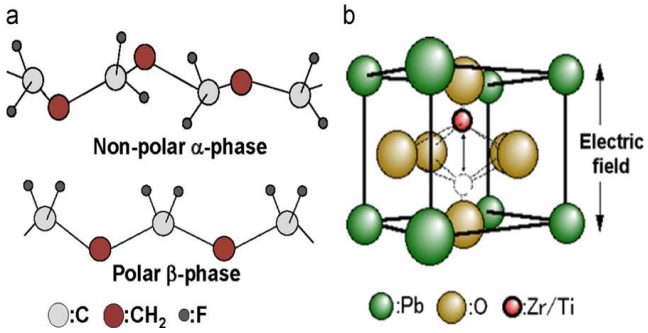

Fig. 4. (a) Schematic diagrams showing crystalline structures of PVDF:(top)non-polar α-phase, and (bottom) polar β-phase. (b)Schematic diagrams showing crystalline structures of PZT. An electric polarization of PZT can shift up/down of Zr/Ti atom and remain their positions after applying and removing an external electric field for the piezoelectric property.

PZT is another good piezoelectric material with its crystalline structure illustrated in **Fig. 4(b)**. An electric polarization of PZT can shift up/down of Zr/Ti atom and remain their positions after applying and removing an external electric field for the piezoelectric property. In their bulk or thin film format. PZT can generate higher voltage as compared with other piezoelectric materials for sensing and actuation and energy harvesting applications. As a ceramic material, bulk PZT is more fragile in comparison to organic PVDF, but has demonstrated very good mechanical strength in nanowire form. During the typical commercial piezoelectric PVDF thin-film production process, a high electrical potential land mechanical stretching is applied at a raised temperature for enhanced piezoelectricity. PVDF nanofibers fabricated by the conventional electrospinning process are under a high bias voltage (410 kV) which could transform some non-polar α-phase structures to polar β-phase structures for piezoelectricity. The near field electrospinning (NFES) process is shown in **Fig. 5**.

It possesses the inherent high electric field with in-situ mechanical stretching for possible alignment of dipoles along the longitudinal direction of the nanofiber.

The PVDF nanofiber network was fabricated using a modified far-field electrospinning process) to align individual nanofibers on to a Kapt on film. Experimentally, a single PVDF nanofiber based nanogenerator was able to generate 0.5–3nA of current and 5–30mV of voltage under repeated long term reliability tests without noticeable performance degradation.

The nanoscale fibers preserve and even enhance piezoelectric properties, and the potential applications are wide-ranging. Sensors built upon the PZT nanofiber technology can be used to monitor aircraft or bridges for structural fatigue in real time. Because the sensors can also

harvest and store energy, they could power themselves indefinitely, eliminating the need for external power or a battery. Mechanical energy could potentially be gathered from heartbeats or body motion to create a self-powering pacemaker. In the future, clothes woven with a combination of thermoelectric and piezoelectric fibers could harvest energy from movement for athletic or military applications.

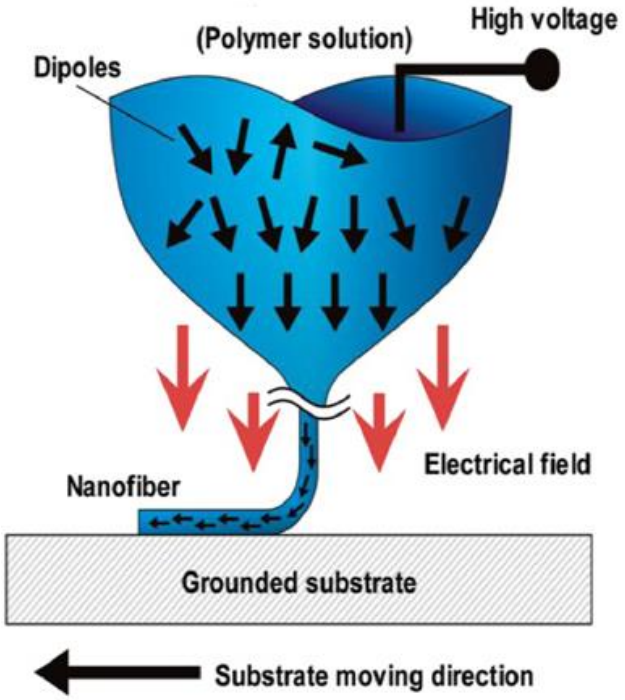

Fig. 5. Schematic diagram of the near-field electrospinning process showing possible dipole directions (black arrows) and electrical filed direction (red arrows). PVDF polymer solution experiences mechanical stretching and in-situ electrical poling during the formation of nanofibers due to the high electrostatic field toward the substrate.

The PZT [**33**] nanofibers are well-suited to sensing and actuating applications because of their unique structure. They are composed of several elements in ion form (having a net positive or negative electrical charge). When force is applied, the positions of the elements shift, releasing electricity, which can be measured to establish the sensing capability. Conversely, researchers can apply electricity, forcing the ions and the structure itself to move, thus establishing the actuating functionality. This advance will unlock numerous opportunities for commercialization of PZT technology. It dramatically enhances the science of piezoelectric materials and builds a new foundation for future research. PZT nanotubes containing nanofibers with electrodes on their internal/external surfaces act as standalone actuators and sensors. They can change their position, morphology or configuration in response to an electric field, mimicking the micro-environment of a cell in vitro and potentially promoting cell growth or aiding in the repair of a damaged neuro-network.

PZT nanofibers were also successfully produced by a sequence of electrospinning and sintering processes. Processing conditions, especially the aging of the precursor solution, were found to be critical to the morphology of the green fiber mats [**36**]. Aging was observed to lead to increased viscosity and a correlated increase in green fiber diameter. Moreover, the annealing regime was found to have a significant influence on the morphology of the sintered nanofiber mats, with slow heating leading to a more uniform morphology. 3–3 composites were prepared from the PZT fiber mats, at about 10% fiber volume fraction, by infiltrating a polyvinylester polymer into the mat. The dielectric constant of the composite measured at room temperature is more than an order of magnitude higher than the polymer matrix and reasonably agrees with the prediction from the rule of mixtures.

Ferroelectric sodium potassium niobate (NKN) was patented as a biocompatible material for implants. Thorough toxicology test showed there were no any bacterial products (endotoxin) appear as well as viability of human monocytes was not negatively affected by the presence of NKN ceramics. Dense homogeneous textile composed from continuous bead-free sodium potassium niobate nanofibers 100 lm long and 50-200 nm in diameter was sintered by sol-gel calcinations assisted electrospinning [**37, 38**]. High resolution electron microscopy and x-ray diffraction revealed preferential cube-on-cube growth of fibers in [001] direction. Raman spectrum of NKN fibers contains all the features characteristic to electrically poled orthorhombic phase. Spontaneous polarization inside highly crystalline nanofiber exists at room temperature though big distance between fibers prevents the settling of a net macroscopic polarization.

Hossain and Kim [**39**] found that the diameters of $PbZrTiO_3$ (PZT) ferroelectric nanofibers decreased with increasing concentration of acetic acid in the sol. Alkoy et al. [**40**] studied the formation of PZT nanofibers using polyvinylpyrrolidone (PVP) as the polymer. They optimized the PVP concentration to 28 wt%; at low concentrations (6 or 12 wt%) fibers were not formed, while at 22 and 34 wt% beads were formed on the nanofi bers. More importantly, they studied the effect of aging of the 28 wt% precursor solution and observed that the fiber diameter increased with increased aging period because the viscosity of the solution increased. Thus, the PVP concentration of the solution was important to obtain bead-free fibers, while the viscosity was the real controlling factor for the diameter. It is also consistent with the observations of McCann et al. [**41**] and Hossain and Kim; [**39**] increasing the precursor concentration or decreasing the acetic acid concentration will increase the viscosity, leading to thicker fibers.

A useful feature of electrospinning is that the collection of the nanofibers can be controlled by the electrode setup McCann et al. [**41**] demonstrated how uniaxially aligned arrays of BaTiO3 nanofi bers can be fabricated by electrospinning onto a collector with an insulating air gap. Such structuring of the nanofibers will be important for using the 1D nanostructure in actual devices.

Hollow $BaTiO_3$ fibers have been prepared by coelectrospinning a Ba-Ti sol with an immiscible heavy mineral oil phase in the inner capillary of a co-axial double capillary setup. The oily core was subsequently extracted with cyclohexane to yield a hollow fiber which was dried and calcined at 1000°C to obtain well-crystallized $BaTiO_3$ fibers. After the electrospinning process, the nanofi bers have to be calcined for crystallization. Adjusting the

calcination temperature may be very important to avoid secondary phases and obtain pure perovskite phase. This is especially relevant for $BaTiO_3$ nanofibers, as $BaCO_3$ typically is formed at lower calcinations temperatures (550–600 °C). Calcination of $BaTiO_3$ is, in general, conducted at a higher temperature than for $PbTiO_3$ /PZT to obtain the perovskite phase. The high stability of $BaCO_3$ is also a challenge in any low-temperature synthesis of Ba-containing perovskites [**42**].

Highly textured (f(00l) > 0.9) polycrystalline Potassium Strontium Niobate ($KSr_2Nb_5O_{15}$) ceramic fibers were drawn and sintered in the polar [001] crystallographic direction by a combination of alginate gelation and templated grain growth methods [**43**]. The microstructure of the textured ceramic fibers showed an orientation of needle-like grains parallel to the fiber drawing direction. Increasing the sintering time resulted in increasing texture and growth of template particles at the expense of the fine matrix grains.

Applications of ferroelectric nanofibers

Using piezoelectric nanofibers as the building blocks in nano-generators and nano-sensors makes them promising candidates for energy harvesting [**43-46**]. X. Chen et al. designed and fabricated a high efficiency nanogenerator based on $Pb(Zr,Ti)O_3$ nanofibers which produced 1.6V output [**45**]. Recently, a Pb-free piezoelectric ceramics system $Ba(Ti_{0.80}Zr_{0.20})O_{3-x}$ $(Ba_{0.70}Ca_{0.30})TiO_3$ (abbreviated as BZT-x BCT, x= molar fraction of BCT) reported by W. Liu et.al Demonstrated a high piezoelectric coefficient d33 about 600 pC/N in Morphotropic Phase Boundary (MPB) region at x= 50 [**47**]. Regarding to its high piezoelectric performance it would be a promising candidate to use as a piezoelectric segment in generators and sensors.

3D and fibrous structures of the electrospun ferroelectric nanofibers in addition to their response to the external electric field and ultrasound vibrations enhanced the tissue and neural tissue regeneration [**48, 49**]. Sodium potassium niobate composition has been studied intensively since it was discovered in 1949 [**46**] and showed a good potential as a biocompatible ferroelectric material [**50-51**]. Biocompatible and ferroelectric $(Na,K)NbO_3$ nanofibers were synthesized with 3D structure that make them a promising candidate as scaffolds for engineering, repair, and regeneration of damaged tissue. $(Ba0.85Ca_{0.15})(Ti_{0.9}Zr_{0.1})O_3$ (BCTZ) piezoelectric and ferroelectric nanofibers were fabricated successfully at 80 ^{0}C with high aspect ratio in morphotropic phase boundary region which can be used as piezoelectric nanogenerator in nano-devices. The ability of piezoelectric ceramics to convert electrical energy to mechanical (and vice versa) makes them valuable in the application of micro-electromechanical systems (MEMS) [**54**]. Although PZT has commonly been used as bulk or thin film, presently PZT fibers are attracting attention due to their anisotropy, excellent flexibility and strength over monolithic PZT ceramics for high performance hydrophones, ultrasonic transducer and smart material applications where damping and reinforcement are combined [**55-57**].

Nanoscale actuators and vibration sensors are required in many applications and these requirements might be satisfied by nanoscale piezoelectric materials. In addition, these nanoscale materials also have the potential to be used for energy harvesting for wireless nano- and microdevices. Recent results from several piezoelectric nanowires and nanofibers were very promising in making a great breakthrough. For instance, zinc oxide, [**58-60**] cadmium sulfide, [**61**] Barium titanate, [**62**] and gallium nitride [**63**] nanowires have been utilized in the conversion of mechanical energy to electric energy due to the piezoelectric effect of these materials. These piezoelectric nanowires and nanofibers can potentially be used for energyharvesting devices, high frequency transducers, implanted biosensors, [**64**] vibration absorbers [**65**] and composite force sensors, [**66-74**] etc.

Conclusion

Nanotechnology is the study and development of materials at nano levels. It is one of the rapidly growing scientific disciplines due to its enormous potential in creating novel materials that have advanced applications. This technology has tremendously impacted many different science and engineering disciplines, such as electronics, materials science, and polymer engineering. Nanofibers, due to their high surface area and porosity, find applications as filter medium, adsorption layers in protective clothing, etc. Electrospinning has been found to be a viable technique to produce nanofibers. Ferroelectric oxides with perovskite structure are widely used in various electronic applications that take advantage of their unique ferroelectric, pyroelectric and piezoelectric properties. They are widely used for multi-layer ceramic capacitors (MLCC), transducers, actuators and ferroelectric random access memories (FRAM). An in-depth review of research activities on the development of ferroelectric nanofibers, fundamental understanding of the electrospinning process, and properties of nanostructured fibrous materials and their applications is provided in this article. A detailed account on the varoius ferroelectric nanofibers that have been electrospun is also elaborated. It is hoped that the overview article will serve as a good reference tool for nanoscience researchers in the field working in ferroelectric systems. Furthermore, this article will help with the planning of future research activities and better understanding of nanofiber characteristics and their applications.

Reference

1. Intelligent Nanomaterials, Wiley, USA, ISBN978-04-709387-99, **2012**.
2. Tiwari, A.; Sharma, Y.; Hattori, S.; Terada, D.; Sharma, A.K.; Turner, A.P.F.; Kobayashi, H. *Biopolymers*. **2010**, 82, 1725. **DOI**: 10.1002/bip.22170
3. Sharma, Y.; Tiwari, A.; Hattori, S.; Sharma, A.K.; Ramalingam, m.; Kobayashi, H. *International Journal of Biological Macromolecules.* **2012**, 51, 627. **DOI**: 10.1016/j.ijbiomac 2012.06.014
4. Teo, W.E.; Ramakrishna, S. *IOP Science* **2006**, 17, R89. **DOI:** 10.1088/0957-4484/*17*/14/R01
5. Nasser, A. M.; Barakat, M. F.; Abadir, A. F.; Mustafa A. K.; Parkb, S.J; Kim, H. Y. *Chemical Engineering Journal*, **2010**, 156, 487. **DOI:** 10.1016/j.cej.2009.11.018
6. Subbiah, T; Bhat, G. S.; Tock, R.W.; Parameswaran, S; Ramkumar, S. S. *Journal of Applied Polymer Science*, **2005**, 96, 557. **DOI**: 10.1002/app.21481

7. Ramaseshan, R; Sundarrajan, S; Jose, R., *J of Applied Physics*, **2007**, 102, 111101. **DOI:** 10.1063/1.2815499
8. Hossain, M; Kim, A. *Materials Letters*, **2009**, 63, 789. **DOI:** 10.1016/j.matlet.2009.01.005
9. Lord Rayleigh, FRS., *Phil. Mag. Series 5*, 2009, 14, 184. **DOI:** 10.1080/14786448208628425
10. Formhals A. US Patent, Process and apparatus for preparing artificial threads. 1, 975, 504, October 2, 1934. **DOI:** 10.2147%2FIJN.S25297
11. Zeleny, J. *Phys. Rev*. **1917**, 10, 1. **DOI:**10.1103/*PhysRev*.10.1
12. Taylor, G. Proc. R. Soc. A **1964**, 280, 383. **DOI** 10.1098/rspa.1964.0151
13. Li, D; Zia, Y. *Advanced Materials.* **2004**, 16, 1151. **DOI:** 10.1002/adma.200400719
14. Shin, Y. M; Hohman, M. M; Brenner, M. P; Rutledge, G. C. *Appl. Phys. Lett*., **2001**, 78, 1149. **DOI:**10.1063/1.1345798
15. Doshi, J; Reneker, D. H. *Journal of Electrostatic.* **1995**, 35, 151. **DOI:**10.1016/0304-3886(95)00041-8
16. Reneker, D. H; Chun, I. *Nanotechnology* **1996**, 7, 216. **DOI:**10.1088/0957-4484/7/3/009
17. Jeun, Joon-Pyo; Kim, Yun-Hye, Lim; Youn-Mook, Choi; Jae-Hak, Jung; Chan-Hee, Kang; Phil-Hyun, Nho; Young-Chang, *J. Ind. Eng. Chem*. **2009**, 15, 430. **DOI**: 10.1016/j.jiec.2009.02.001
18. Ramakrishna, S; Fujihara, K; Eong, W; An Introduction to Electrospinning And Nanofibers, World Scientific Press, ISBN: 978-981-256-415-3, **2005**.
19. Teo, W. E; Inai, R; Ramakrishnan, S. *Science and Technology Adv. Mater.* **2011**, 12, 013002. **DOI:** 10.1088/1468-6996/12/1/013002
20. Larrondo, L; John, St. M. R.. *J Polym Sci Polym Phys Ed* **1981**, 19, 921. **DOI:** 10.1002/jbm.a.30673
21. Subbiah, T; Bhat, G. S; Tock, R. W; Parameswaran, S, Ramkumar, S. S. *J Appl Polym Sci* **2005**, 96, 557. **DOI:** 10.1002/app.21481
22. Fenn, J. B; Mann, M; Meng C. K; Wong, S. F; Whitehouse, C. M. *Science* **1989**, 246, 64. **DOI:** 10.1126/science.2675315
23. Hohman, M. M; Shin, M; Rutledge, G; Brenner, M. P. *Phys Fluids.* **2001**, 13, 2201. **DOI:** 10.1063/1.1383791
24. Hunley, M. T; Long, T. E. *Polym Int* **2008**, 57, 385. **DOI:**10.1002/pi.2320
25. Zhang, X; Kotaki, M; Okubayashi, S; Sukigara, S. *Acta Biomaterialia* **2010**, 6, 123. **DOI:** 10.1016/j.actbio.2009.06.007
26. Zong, X; Kim, K; Fang, D; Ran, S; Hsiao, B. S; Chu, B. *Polymer* **2002**, 43, 4403. **DOI:** 10.1016/S0032-3861(02)00275-6
27. Tuck, S. J; Leach, M. K; Feng, Z. Q; Corey, J. M. *Materials Science and Engineering: C* **2012**, 32, 1779. **DOI:** 10.1016/j.msec.2012.04.060
28. Dhakate, S. R; Singla, B; Uppal, M; Mathur, R. B. *Adv. Mat. Lett.* **2010**, 1, 200. **DOI:** 10.5185/amlett.2010.8148
29. Yuh, J; Perez, L; Sigmund, W. M; Nino, J. C. *Physica E* **2007**, 37, 254. **DOI:** 10.1016/j.physe.2006.09.013
30. Li, H; Wu, H; Lin, D; Pan, W. *J. Am. Ceram. Soc.* **2009**, 92, 2162. **DOI:** 10.1111/j.1551-2916.2009.03177.x
31. Li, Y; Gao, X. P; Li, G. R; Pan, G. L; Yan, T. Y; Zhu, H. Y. *J. Phys. Chem.* C. **2009**, 113, 4386. **DOI:** 10.1021/jp810805f
32. Rørvik , P. M; Grande , T; Einarsrud, M. A. *Adv. Mater.* **2011**, 23, 4007. **DOI:** 10.1002/adma.201004676
33. Meyer, R; Shrout, T; Yoshikawa, S. *J. Am. Ceram. Soc* **1998**, 81, 861. **DOI:** 10.1111/j.1151-2916.1998.tb02420.x
34. Y. Li, X. P. Gao, G. R. Li, G. L. Pan, T. Y. Yan, and H. Y. Zhu, *J. Phys. Chem.C.* **2009**, 113, 4386. **DOI:** 10.1021/jp810805f
35. Zhang, H; Long, Y; Li, Z; Sun, B; Sheng, C. *Advanced Mat Research.* **2012**, 418, 684. **DOI:** 10.4028/www.scientific.net/AMR.418-420.684
36. Jalalian, A; Grishin, A. M. *Applied Physics Letters.* **2012**, 100, 012904. **DOI:** 10.1063/1.3673282
37. Maxim, F; Ferreira, P; Vilarinho , P. M; Reaney, I. *Cryst. Growth Design.* **2008**, 8, 3309. **DOI:** 10.1021/cg800215r
38. Jalalian, A; Grishin, A. M. *Applied Physics Letters* 2012, 100, 012904. **DOI:** 10.1063/1.3673282
39. Hossain, M; Kim , A. *Mater. Lett* **2009**, 63, 789. **DOI:** 10.1016/j.matlet.2009.01.005
40. Alkoy, E. M.; Dagdeviren, C; Papila, M. *J. Am. Ceram. Soc.* **2009**, 92, 2566. **DOI:** 10.1111/j.1551-2916.2009.03261.x
41. McCann , J. T; Chen , J. I. L; Li , D; Ye , Z. G.; Xia , Y. *Chem. Phys. Lett.* **2006** , 424 , 162. **DOI:** 10.1016/j.cplett.2006.04.082
42. Maxim, F; Ferreira, P; Vilarinho , P. M; Reaney, I. *Cryst. Growth Design* 2008, 8, 3309. **DOI:** 10.1021/cg800215r
43. Alkoy, S; Dursun, S. *J. Am. Ceram. Soc*. **2012**, 95, 937. **DOI:**10.1111/j.1551-2916.2011.04994.x
44. Chen, C. Y; Huang, J. H; Song, J; Zhou, Y; Lin, L; Huang, P. C; Zhang, Y; Liu, C. P; He, J. H; Wang, Z. L, *ACS NANO* **2011,** 5, 6707. **DOI:** 10.1021/nn202251m
45. Que, R; Shao, M; Wang, S; Ma, D. D. D; Lee, S. T. *Nano lett.* **2011,** 11, 4870. **DOI:** 10.1021/nl2027266
46. Chen, X; Xu, S; Yao, N; Shi, Y. *Nano let.* **2010**, 10, 2133. **DOI:** 10.1002/ pssr.201105120
47. Liu, W; Ren, X. *Phys. Rev. Lett.* **2009**, 103, 257602. **DOI:** 10.1063/1.3629784
48. Weber, N; Lee, Y. S; Shanmugasundaram, S; Jaffe, M; Arinzeh ,T. L. *Acta Biomater*. **2010**, 6, 3550. **DOI:** 10.1016/j.actbio.2010.03.035
49. Jianqing, F; Huipin ,Y; Xingdong, Z. *Biomaterials* **1997**, 18, 1531. **DOI:** 10.1063/1.4729619
50. Matthias, B. T. *Phys. Rev*. **1949**, 75, 1771. **DOI:** 10.1063/1.3512980
51. Hagh, N. M; Jadidian, B; Safari, A. *J. Electroceram*. **2007** 18, 339. **DOI:**10.1063/1.2897033
52. Cho, C. R; Grishin, A. M. *Appl. Phys. Lett.* **1991,** 75, 268. **DOI:** 10.1063/1.124344
53. Nilsson, K; Lidman, J; Ljungstrom, K; Kjellman. U.S. patent **2003**, 6, 526, 984.
54. Hsu, Y. C.; Wu, C. C.; Lee, C. C.; Cao, G. Z.; Shen, I. Y. *Sens Actuator A* **2004,** 116, 369. **DOI:** 10.1016/j.sna.2004.05.024
55. Dent, A. C.; Nelson, L. J; Bowen, C. R.; Stevens, R; Cain, M; Stewart, M. *J Eur Ceram Soc* **2005**, 25, 2387. **DOI:** 10.1007/s10853-011-5345-7
56. Steinhausen, R; Hauke, T; Seifert, W; Beige, H; Watzka, W; Seifert, S; et al. *J Eur Ceram Soc* **1999**, 19, 1289. **DOI:** 10.1016/S0167-577X(03)00302-1
57. Zhang, M; Miranda Salvado, I.M.; Vilarinho, P. M. *Materials Letters* **2003** 57 4271. **DOI:** 10.1016/S0167-577X(03)00302-1
58. Wang, Z. L; Song, J. H. *Science* **2006,** 312, 242. **DOI:** 10.1126/science.1124005
59. Wang, X. D, Song, J. H.; Liu, J; Wang, Z. L. *Science.* **2007**, 316, 102. **DOI:** 10.1038/ncomms1098
60. Qin, Y; Wang, X. D; Wang, Z. L. *Nature London.* **2008**, 451, 809. **DOI:** 10.1038/nature06601
61. Lin, Y. F; Song, J. H; Ding, Y; Lu, S. Y; Wang, Z. L. *Appl. Phys. Lett.* **2008**, 92, 022105. **DOI:** 10.1063/1.2831901
62. Wang, Z. Y; Hu, J; Suryavanshi, A. P; Yum, K; Yu, M. F. *Nano Lett.*, **2007**, 7, 10. **DOI:** 10.1021/nl062140y
63. Su, W. S; Chen, Y. F; Hsiao, C. L; Tu, L. W. *Appl. Phys. Lett*. **2007**, 90, 063110.

DOI: 10.1063/1.2472539
64. Lieber, C. M; Wang, Z. L. *MRS Bull* **2007**, 32, 99. **DOI:** 10.1557/mrs2007.41
65. Davis, C.L.; Lesieutre, G.A. *J. Sound Vib*. ***2000***, 232, 601. **DOI:** 10.1006/jsvi.1999.2755
66. Choy, S. H; Chan, H. L. W; Ng, M. W; Liu, P. C. K; *Appl. Phys. A*, **2005**, 81, 817. **DOI:** 10.1007/s00339-004-2874-9
67. Pandey, S. K; James, A. R; Raman, R; Chatterjee, S. N, *Physica B*, **2005**, 369, 135. **DOI:** 10.1016/j.physb.2005.08.024
68. Berlincourt, D; Krueger, H. H. A, Morgan Electro Ceramics Company, Technical Publication TP-226.
69. Yang, R. S; Qin, Y; Dai, L. M; Wang, Z. L. *Nat. Nanotechnol.* **2009**, *4*, 34. **DOI:** 10.1038/nnano.2008.314
70. Yang, R. S; Qin, Y; Li, C; Zhu, G; Wang, Z. L. *Nano Lett.* **2009**, *9*, 1201. **DOI:** 10.1021/nl803904b
71. Wang, Z. L; Song, J. H. *Science* **2006**, *312*, 242. **DOI:** 10.1126/science.1124005
72. Wang, X. D; Song, J. H; Liu, J; Wang, Z. L. *Science* **2007**, *316*, 102. **DOI:** 10.1038/ncomms1098
73. Qin, Y; Wang, X. D.; Wang, Z. L. *Nature* **2008**, *451*, 809. **DOI:** 10.1038/NNANO.2010.46
74. Xu, S; Qing, Y; Xu, C; Wei, Y. G; Yang, R. S; Wang, Z. L. *Nat.Nanotechnol.* **2010**, *5*, 367. **DOI:** 10.1021/nl100812k | Nano Lett

